Optimization of Noah and Noah_MP WRF Land Surface Schemes in Snow-Melting Conditions over Complex Terrain

ELENA TOMASI, LORENZO GIOVANNINI, DINO ZARDI, AND MASSIMILIANO DE FRANCESCHI

Atmospheric Physics Group, Department of Civil, Environmental and Mechanical Engineering, University of Trento, Trento, Italy

(Manuscript received 25 October 2016, in final form 14 September 2017)

ABSTRACT

The paper presents the results of high-resolution simulations performed with the WRF Model, coupled with two different land surface schemes, Noah and Noah_MP, with the aim of accurately reproducing winter season meteorological conditions in a typical Alpine valley. Accordingly, model results are compared against data collected during an intensive field campaign performed in the Adige Valley, in the eastern Italian Alps. In particular, the ability of the model in reproducing the time evolution of 2-m temperature and of incoming and outgoing shortwave and longwave radiation is examined. The validation of model results highlights that, in this context, WRF reproduces rather poorly near-surface temperature over snow-covered terrain, with an evident underestimation, during both daytime and nighttime. Furthermore it fails to capture specific atmospheric processes, such as the temporal evolution of the ground-based thermal inversion. The main cause of these errors lies in the miscalculation of the mean gridcell albedo, resulting in an inaccurate estimate of the reflected solar radiation calculated by both Noah and Noah_MP. Therefore, modifications to the initialization, to the land-use classification, and to both land surface models are performed to improve model results, by intervening in the calculation of the albedo, of the snow cover, and of the surface temperature. Qualitative and quantitative analyses show that, after these changes, a significant improvement in the comparability between model results and observations is achieved. In particular, outgoing shortwave radiation is lowered, 2-m temperature maxima increased accordingly, and ground-based thermal inversions are better captured.

1. Introduction

Accurate predictions of meteorological variables over complex terrain are a particularly challenging task for numerical weather models. On one hand, the resolution of the numerical simulation has to be sufficiently fine to adequately describe relevant topographic features. Yet original topography datasets often have to be smoothed, to prevent numerical instability problems when using terrain-following coordinates (Zängl 2012). On the other hand, complex terrain strongly influences meteorological fields, especially in the lowest layers, where energy and mass fluxes between the ground and the atmosphere regulate temperature and wind regimes within the boundary layer. This requires numerical weather prediction models to include appropriate parameterizations, accurately reproducing small-scale processes and land surface interactions with the atmosphere. In particular, calculations of the energy and mass transfer at the ground interface are performed by land surface models (LSMs), which provide bottom boundary conditions to the atmospheric model. Many different LSMs have been developed, refined, and tested over the past decades (Oleson et al. 2013; Xue et al. 1991; Noilhan and Planton 1989), but great uncertainty still affects their results (Dirmeyer et al. 2006; Zhang et al. 2013). Particularly challenging for LSMs is the calculation of surface fluxes over snow-covered surfaces. Indeed, snowpack strongly alters energy and mass balances, influencing surface heat fluxes, ground temperature, runoff, and soil moisture. Several studies (e.g., Barlage et al. 2010; Jin et al. 2010) highlighted that LSMs often poorly simulate snow water equivalent and its evolution in time, and that this can directly influence atmospheric feedbacks (e.g., Qu and Hall 2006; Jin and Miller 2007). For this reason, it is essential to keep evaluating and improving LSMs performance with particular care for the snow cover treatment.

The present work focuses on two of the LSMs available within the Weather Research and Forecasting (WRF) Model (Skamarock et al. 2008): the Noah (Chen and Dudhia 2001; Chen et al. 1996; Ek et al. 2003) and the Noah_MP (Niu et al. 2011; Yang et al. 2011) schemes.

Corresponding author: Elena Tomasi, elena.tomasi@unitn.it

DOI: 10.1175/MWR-D-16-0408.1

The Noah model represents probably the most widely used land surface scheme among the WRF community, being applied in the research field and in different weather and regional climate models [e.g., the operational North American Mesoscale Forecast System (NAM) run by the National Centers for Environmental Prediction (NCEP)]. It can be considered the combination of different physical approaches (Chen and Dudhia 2001), each describing one of the processes influencing energy and mass fluxes at the ground. The Mahrt and Ek (1984) approach is used for potential evapotranspiration, and the Simple Water Balance method by Schaake et al. (1996) is applied for the runoff calculation. In addition, the multilayer soil model by Mahrt and Pan (1984), the simple canopy model by Pan and Mahrt (1987), extended by Chen et al. (1996), and a single layer snowpack scheme (Koren et al. 1999; Livneh et al. 2010) are implemented in the Noah LSM.

The Noah_MP model represents an evolutional version of Noah LSM, including structural changes and multiparameterization (MP) options in order to improve model performance, allowing physically based ensembles and selection of optimal scheme combinations (Niu et al. 2011). This approach introduces a great variety of options in the application of the model, as the user is given nearly 5000 possible combinations (Yang et al. 2011) of different schemes, but even in its standard version (i.e., with a fixed set of parameterizations) Noah_MP represents an augmented version of Noah LSM. In particular, vegetated and bare portions of cells are treated separately, snow cover is described with a three-layer model, the vegetation canopy is dynamically treated, and a simple groundwater model is introduced.

The aim of this paper is to test and improve these LSMs' performance over complex terrain, in snowmelting conditions. To achieve this objective, we compare results of simulations run with WRF coupled with both LSMs, testing their abilities in reproducing 2-m temperature as well as incoming and outgoing surface short- and longwave radiation, over complex terrain and at a local scale. Simulations are conducted in early February 2006, when melting snow was covering both the valley floor and the sidewalls at the target site, in the Adige Valley. This situation represents a challenging task for the LSMs, which are tested in a transitional phase between different ground thermal regimes, when the proper description of snowpack depletion is essential. Indeed, the ability of Noah and Noah_MP to reproduce snow-related variables has already been compared in Niu et al. (2011), but the assessment was performed on short-grass-covered sites only. Nevertheless, land-use type is a relevant parameter, as LSMs are usually very sensitive to this. In this paper, comparisons are made over apple orchard and broadleaf forest land cover, where Noah and Noah_MP differences are expected to be maximized, because of the differences in the two LSMs in separating vegetated and bare ground and in treating the vegetation canopy. Moreover, after assessing the abilities and deficiencies of the standard model, some modifications to both WRF initialization and LSMs are applied, and their effects on the results are evaluated. Snow cover, land use, and snow-covered surface albedo are found to be relevant variables in the calculation of 2-m temperature, affecting the model's ability to reproduce peculiar phenomena over complex terrain, such as nighttime ground-based thermal inversions (i.e., cold air pooling).

The paper is organized as follows. Section 2 briefly introduces the area of interest, the experimental dataset used for the validation process, and the period of study. Section 3 describes the methodology and the modeling setup of the presented simulations, focusing on the modifications applied. In section 4 numerical results are presented and compared with observations for the standard and modified model setup: a qualitative evaluation is conducted, together with a statistical analysis of the model performance. A discussion on the effects of the modifications implemented is presented in section 5. Finally, section 6 contains a summary of the results and some conclusions.

2. Study area and experimental dataset

a. Study area

The target area for the present work is the lower part of the Adige Valley, in the eastern Italian Alps (Fig. 1a). The portion of the valley analyzed in this paper is about 45 km long, 2 km wide, and mainly north–south oriented. The valley floor elevation ranges between 150 m above mean sea level (MSL) in the southern part, up to 200 m MSL in the northern part, and the surrounding mountain peaks range between 1500 and 2000 m MSL. The sidewalls are mostly very steep, especially in the northwestern side of the valley. The study area includes the cities of Trento and Rovereto and other minor urbanized centers, including the town of Aldeno, where the intensive field campaign, whose measurements are used in this work, was performed (Fig. 1b). Except for these urban areas, the valley floor is mainly devoted to agriculture (apple orchards), while most of the sidewalls are covered with deciduous broadleaf and evergreen needleleaf forests.

b. Experimental dataset

In the present work two different datasets are used. The first dataset comes from an intensive measurement campaign carried out in 2006, near the town of Aldeno, Italy, within the Monitoring and Minimisation

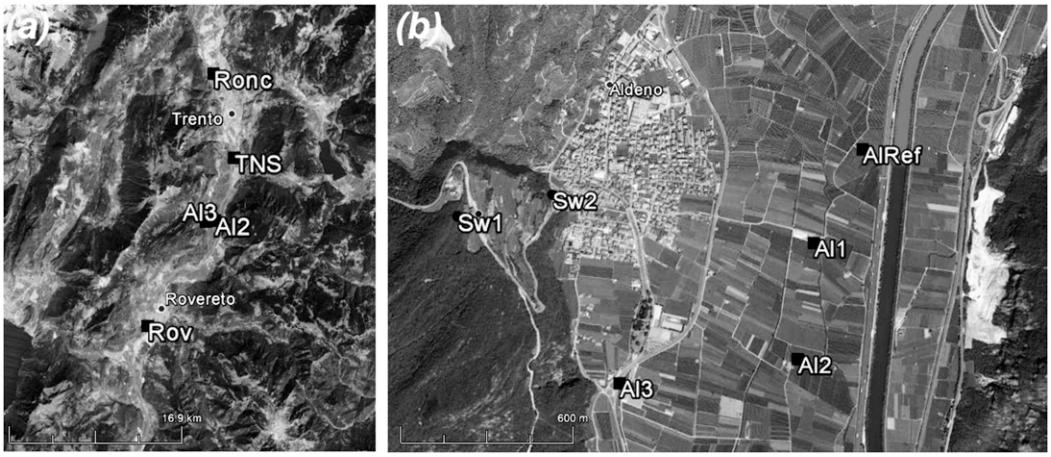

FIG. 1. Topography of the lower part of the Adige Valley: (a) study domain with the cities of Trento and Rovereto, the town of Aldeno, and the permanent weather stations used in this paper; (b) zoom-in on the town of Aldeno with the measurement stations of the ALPNAP project (squares for valley floor stations and dots for sidewall stations; background map from Google Earth).

of Traffic-Induced Noise and Air Pollution Along Major Alpine Transport Routes project (ALPNAP; Heimann et al. 2007): a complete description of the ALPNAP field instrumentation can be found in de Franceschi and Zardi (2009) (M. de Franceschi and D. Zardi 2006, unpublished manuscript). The present work utilizes observations from 1) a meteorological station and a four-channel net radiometer located on the valley floor (AlRef), which is used as the reference observation site to evaluate model results; 2) a conventional weather station on the valley floor (Al1); and 3) two portable thermohygrometers located on the western sidewall at different elevations (Sw1 and Sw2), respectively at 390 and 240 m MSL (Fig. 1b). The 2-m temperature measurements were recorded at all the observation sites, while incoming and outgoing shortwave (SW) and longwave (LW) radiation measurements are available only for the reference station (AlRef). This dataset provides a fairly complete view of the evolution of the principal meteorological variables on the valley floor close to Aldeno, including incoming and outgoing SW and LW radiation, which are of fundamental importance for the evaluation of land surface model results. Moreover, the thermohygrometers on the western valley sidewall allow the evaluation of the development of ground-based thermal inversions.

The second dataset comprises measurements from five permanent weather stations on the valley floor (Al2, Al3, Ronc, TNS, and Rov), operated by Meteotrentino (i.e., the local meteorological office), and by the Edmund Mach Foundation (2013, unpublished manuscript). Measurements of 2-m temperature from these weather stations are also used to validate model results farther away from the town of Aldeno, along the Adige Valley floor. All data used in the present work are hourly averages.

c. *Study period*

For the purpose of the present work, 4 days were selected out of the ALPNAP measurement campaign in Aldeno (viz., 12–15 February 2006) for their interesting meteorological conditions. First of all a transition from clear sky to cloudy conditions, occurred between the third and the last day of simulation; second, a ground-based thermal inversion developed during nighttime, breaking up in the central hours of the day, with strong temperature differences between the valley floor and the sidewalls; third, 15-day-old snow was covering the ground, after a snowfall at the end of January 2006.

3. Methodology and model setup

In the present paper, the results of four different simulations are presented. Simulations 1 and 2 aim at testing the standard versions of the Noah and of the Noah_MP LSMs, respectively, released with WRF 3.8.1. Results of these simulations are used to evaluate the performance of the standard version of the model when applied at a high resolution, as it might be done by a common user. After evaluating the results of the standard simulations, in order to improve model performance, some corrections were implemented to the initialization of the model, to the land-use classification and to both the LSMs. Simulations 3 and 4 were performed with all these changes, using the modified versions of Noah and Noah_MP, respectively.

Except for the use of the two different LSMs, all the simulations share the same settings as to domain

TABLE 1. List of nested domain characteristics.

Nest No.	Horizontal grid space (km)	Dimensions (km × km)	Time resolution (s)
1	10.8	1080 × 1080	5
2	3.6	327.6 × 327.6	1.6
3	1.2	109.2 × 120	0.55
4	0.4	36.4 × 43.6	0.19

dimensions, horizontal and vertical grid spacing, meteorological boundary/initial conditions, static input data, and all the physics options. In the following sections the basic settings regarding all the simulations are presented and the modifications implemented in simulations 3 and 4 are described.

a. Model setup

The horizontal domain used for the simulations consists of four two-way nested domains, with grid spacing ranging from 10.8 km in the external domain to 400 m in the innermost, with a 3:1 ratio between successive nests, while 40 vertical levels are used for the vertical discretization (see Table 1 and Fig. 2 for details). Simulations cover a period of 108 h, starting at 1200 UTC (LST = UTC + 1 h) 11 February 2006 and ending at 0000 UTC 16 February 2006. The first 12 h, being influenced by the model initialization, are not considered for the comparison with observations.

The initial and boundary conditions are supplied by the 6-hourly NCEP Final Operational Global Analysis (FNL) data on 1° grids. Topography and land-use data in the three external domains come from the default WRF datasets, with a resolution of 1 km. The Moderate Resolution Imaging Spectroradiometer (MODIS)-based dataset is used for land cover, with the IGBP Land Cover Type Classification. Nevertheless, these data are not sufficient in order to properly describe the orographic features and the land use in the inner domain; therefore, customized static data with a very high resolution were provided. The adopted topography dataset has an original spatial resolution of 30 m (de Ferranti 2013). One smoothing pass with the 1–2–1 smoothing filter was used to prevent numerical instability. The topography of the simulation domains is shown in Fig. 2. Similarly, the land use also needs to be described with a high resolution in order to obtain a realistic characterization of meteorological phenomena at local scale in the innermost domain. For this reason, the Corine Land Cover (CLC) dataset (European Environment Agency 2006) was adopted for the present simulations. This 100-m resolution dataset was reclassified into the standard IGBP classes, as shown in Giovannini et al. (2014a), in order to match the WRF land-use tables.

All the presented simulations share the same physics schemes, except for the land surface model. The microphysics scheme used is the WRF single-moment 3-class simple ice scheme (Hong et al. 2004), while the parameterization applied for the PBL is the Yonsei University (YSU) scheme (Hong et al. 2006). The Grell–Freitas cumulus scheme (Grell and Dévényi 2002) is employed for the two external domains, while no cumulus physics option is adopted for domains 3 and 4. The Dudhia scheme (Dudhia 1989) and RRTM scheme (Mlawer et al. 1997) are used for SW and LW radiation, respectively. Radiation schemes are called every 10 min and are applied taking into account both the effects of shading and slope angle in complex terrain.

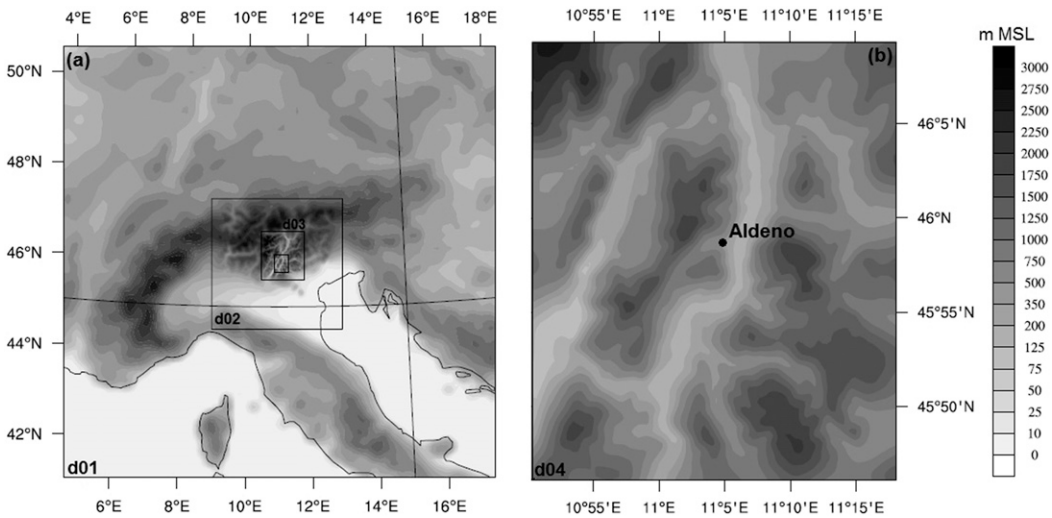

FIG. 2. Elevation contours of the simulation domains: (a) the four simulation domains and (b) the inner domain, centered on the town of Aldeno

Noah_MP LSM is always run with its default combination of internal parameterizations, which include the following: no dynamic vegetation, a Ball–Berry-type stomatal resistance scheme (Ball et al. 1987; Collatz et al. 1991, 1992; Sellers et al. 1996; Bonan 1996), the simple TOPMODEL by Niu et al. (2007) for runoff and groundwater treatment, the Niu and Yang (2006) approach for supercooled liquid water (or ice fraction) and frozen soil permeability, a two stream radiation transfer model applied to vegetated fraction, the CLASS option for ground snow surface albedo (Verseghy 1991), the relatively complex functional form of Jordan (1991) for partitioning precipitation into rainfall and snowfall, and the Sakaguchi and Zeng (2009) option for surface evaporation resistance. In addition, lower boundary conditions of long-term bottom (8-m depth) temperatures come from original Noah reference data, the snow/soil temperature time scheme is semi-implicit, the same soil moisture factor for stomatal resistance as Noah LSM is used, the applied glacier treatment includes phase change of ice and the Monin–Obukhov surface-layer drag coefficients are utilized.

Model output is written every 15 min for all four simulations; the corresponding hourly averages are compared with observations.

b. *Applied modifications*

1) MODIFICATIONS TO WRF INITIALIZATION

As will be shown in section 4, the results of simulations 1 and 2 highlighted that the standard procedure for the initialization of ground-covering snow in the WRF Preprocessing System (WPS) resulted in a consistent overestimation of the snow depth. Unfortunately during the ALPNAP field campaign no snow height measurements were collected, and none of the permanent weather stations along the valley floor performed snow height measurements. However, on the basis of photographs taken during the field campaign, showing the snow condition on the ground, an estimate of the snow depth and of the snow density was made and the overestimation of the model was pointed out. This overestimation was mainly due to assumptions in the WPS, and not simply to the reanalysis.

First, the WRF preprocessor code ungrib doubles the snow water equivalent (SWE) value when using NCEP reanalysis. However, compared to field observations, this operation produced an overestimation of the amount of snow on the ground of almost 20% in the present case study. Second, the snow density, through which ungrib calculates snow height from SWE data, is always assumed by the ungrib code to be that of fresh snow (i.e., 200 kg m^{-3}), no matter the season of the year or the date of the last snowfall. This assumption results in a significant overestimation of snow height. The combination of SWE and snow depth overestimations directly affects the snow fraction and the surface albedo calculated by the LSMs. After estimating both the SWE and the snow height on the ground according to field observations, the ungrib code was modified so that the calculated initial values reproduced a realistic snow condition at the simulation starting time. This was obtained by multiplying the SWE NCEP Global Forecast System (GFS) value by 1.7 times and fixing the 15-day-old snow density to 350 kg m^{-3} (Pomeroy and Brun 2001; Meloysund et al. 2007).

2) MODIFICATIONS TO THE LAND USE

According to the used MODIS-based dataset, the valley floor of the Adige valley is classified, apart from the urban areas, entirely as "cropland," which includes all types of cultivation. However the land-use parameters of the cropland class seemed not appropriate for the present case. In fact, cropland land use refers to typical American crop farming (e.g., corn cultivation), which has little in common with apple orchards. In particular, when snow lies on the ground, the vegetated fraction of a domain cell changes enormously depending on the height of the crop, and is much higher if actual trees (such as apple trees) cover the terrain. For this reason, a new land-use class was introduced and described (in VEGPARM.TBL and MPTABLE.TBL at http://www2.mmm.ucar.edu/wrf/users/download/get_source.html) as a composition of parameters of the class labeled by IGBP as "deciduous broadleaf forest" and of the class labeled by the CLC as "apple orchard": specifically, deciduous broadleaf forest parameters are utilized with locally estimated values for the canopy top and bottom heights, for the minimum and maximum roughness lengths, and for the tree density (Table 2). In the Noah LSM, this modification in the land-use classification produced a significant decrease in the snow cover fraction (SCF) in the interested cells, with significant effects on the cell albedo and, as a consequence, on the 2-m temperature calculation. Moreover, an additional issue in describing the characteristics of land-use classes was identified in the Noah_MP parameters table. Specifically, the Noah_MP model calculates the SCF of a cell following the formulation of Niu and Yang (2007):

$$\mathrm{SCF} = \tanh\left[\frac{h_{\mathrm{sno}}}{2.5 z_{0_g} (\rho_{\mathrm{sno}}/\rho_{\mathrm{new}})^m}\right], \qquad (1)$$

where h_{sno} is the snow depth, fresh snow density ρ_{new} (100 kg m^{-3}) scales the actual snow density ρ_{sno}, z_{0_g} is the ground roughness, and m is a melting factor determining

TABLE 2. Modified parameters in the "deciduous broadleaf forest" class in order to create a new ad hoc "orchard" land-use class.

Parameters	IGBP deciduous broadleaf forest	New orchard
Canopy top height	20	3
Canopy bottom height	11.5	1
Min roughness length	0.5	0.3
Max roughness length	0.5	0.3
Tree density	0.1	0.25

the curves in the melting season. According to Niu and Yang (2007) and Su et al. (2008), this factor is generally larger for larger scale and should be calibrated against observed snow cover fraction or surface albedo. In the Noah_MP scheme, as implemented in WRF 3.8.1, m is fixed to 2.5 for every land-use type. In this study, the factor m was adjusted to the value of 1, on the basis of snow cover fraction data coming from the MODIS/*Terra* Snow Cover Daily dataset (Hall and Riggs 2016), with a resolution of 500 m, and of previously suggested values (Niu and Yang 2007; Su et al. 2008). Equation (1) was indeed applied with the modified initial snow depth and density, and the value of m was calibrated so as to obtain the satellite-observed snow cover fraction. Specifically, with m equal to 2.5 the calculated SCF resulted in a value of about 0.2 in the reference station, while satellite observations suggest a value for SCF at around 0.9, which is reached with m equal to 1.

3) MODIFICATIONS TO THE NOAH LSM

The results of simulation 1 highlighted that the snow-covered cell albedo was systematically overestimated by the Noah LSM, which implements the procedure proposed by Livneh et al. (2010) for calculating snow albedo. However, a closer look at how Livneh's scheme is implemented within the WRF 3.8.1 code highlighted two inconsistencies. Following Livneh et al. (2010), the albedo of the snow-covered portion of the cell (α_{snow}) is calculated as

$$\alpha_{\text{snow}} = \alpha_{\max} A^{t^B}, \tag{2}$$

where t is the age of the snow (in days), A and B are constant parametric coefficients (different for either the accumulation or melting season), and $\alpha_{\max}$ is the maximum albedo of fresh snow, dependent on the land-use class. However, in WRF, the A and B coefficients are fixed to the values for the accumulation period only. In other words, the albedo of the part of the cell covered by snow decays over time at a fixed rate, independently of the season of the year. Moreover, t is always initialized to 0 days (i.e., with a fresh snow cover). Neither of these assumptions are appropriate for the present case, as the snow was progressively melting during the field campaign, and the last snowfall occurred 15 days before the beginning of the study period. Accordingly two changes in to the implementation of the Livneh formulation were introduced: the A and B parametric coefficients were fixed to the melting season values, and the time since the last snowfall, t, was set to 15 days. After these changes the surface albedo in the valley floor resulted in a value almost half of its previous one.

4) MODIFICATIONS TO THE NOAH_MP LSM

After the application of the modifications to the snow cover initialization and to the land-use classification, the Noah_MP model still showed some deficiencies in increasing the 2-m temperature during daytime. A detailed analysis of the Noah_MP LSM implementation within the WRF code revealed that the model intrinsically prevents the ground temperature from exceeding 0°C in the case of a snow depth greater than 5 cm, both under canopy and over bare soil. This assumption determines in turn a strong limitation to the increase of the 2-m temperature. However this restriction appears quite questionable, especially if applied over a thin snow layer, under sun-exposed canopy. It is in fact reasonable to assume that some patches of snow-free ground may emerge under trees when the snow depth is small. For this reason, the implemented limitation in Noah_MP LSM was removed for under-canopy snow depths smaller than 10 cm.

4. Results

In this section results from the standard simulations (1 and 2) and from the modified simulations (3 and 4) are compared and discussed in terms of incoming and outgoing short- and longwave radiation and 2-m temperature. Differences in the results between simulations 3 and 4 and the standard simulations are the effects of all the aforementioned modifications combined together. Section 5 discusses the effects of each modification on the results.

a. Radiation

Figure 3 shows incoming and outgoing shortwave radiation as observed during the 4-day study period and as reproduced by model simulations. Incoming SW radiation is well reproduced by all the simulations, which are also able to identify the cloudy-sky conditions during the fourth day. On the other hand, as expected due to the overestimation of the snow cover and of the snow albedo, the outgoing SW radiation is greatly overestimated by simulations 1 and 2, with higher errors for simulation 1. The proposed modifications significantly

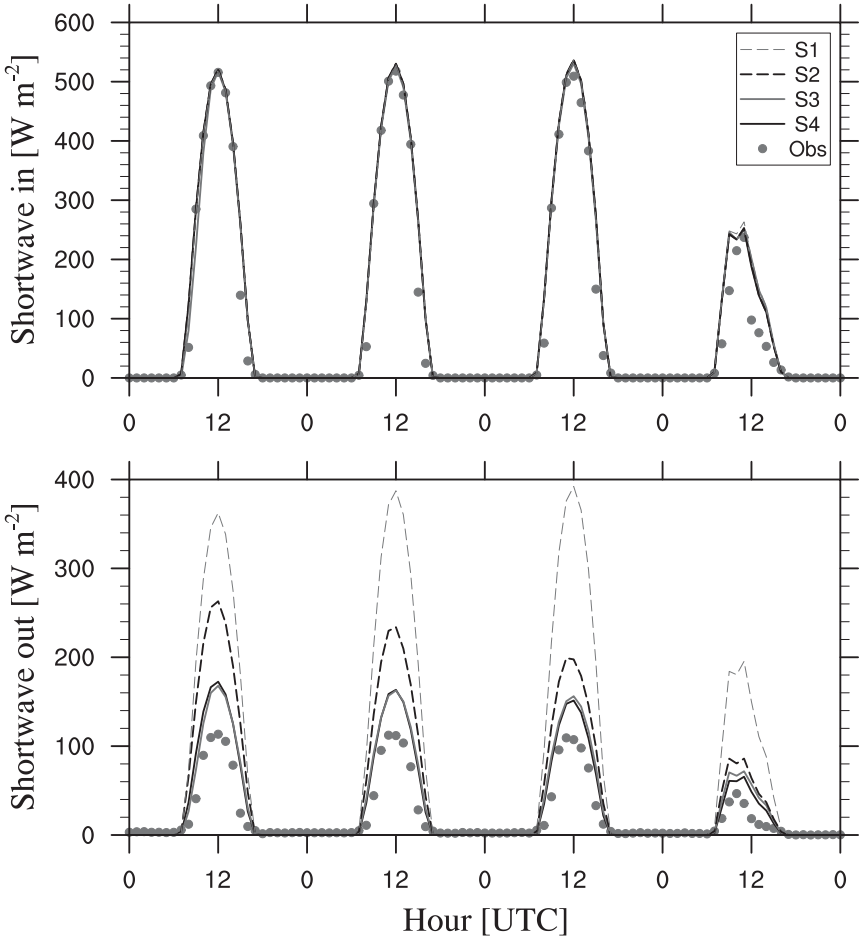

FIG. 3. Incoming and outgoing shortwave radiation observed and estimated by the four simulations (S1–S4) at the valley floor reference station (AlRef).

improve the agreement with observations, with similar results in both simulations 3 and 4. The outgoing SW radiation decreases, at midday peaks, by about ~200 W m^{-2} in simulation 1 and by about ~40–100 W m^{-2} in simulation 2, and the bias between calculated and observed values reduces to a maximum value of ~50 W m^{-2} around midday.

Concerning longwave radiation, Fig. 4 shows that incoming and outgoing LW radiation are basically underestimated by the default WRF runs, especially by simulation 1. The modified simulations allow the incoming and outgoing LW radiation to be increased, reducing the differences with the observed values. It is interesting to notice that both the change of LSM (from Noah to Noah_MP) and the modifications introduced have an influence on the incoming LW radiation. Indeed, modifications of surface temperature in the model affect the temperature of the lower layers of the atmosphere. The incoming LW radiation thus changes, as it directly depends on the temperature of the emitting source. This effect is particularly noticeable in a narrow valley, where an increase in surface temperature on the valley slopes significantly affects radiation budgets in the whole valley atmosphere, increasing the downward LW radiation on the valley floor. Results in terms of incoming LW radiation are similar for simulations 3 and 4: midday peaks are quite well reproduced, whereas the incoming LW radiation is still considerably underestimated after sunset on the second and third days, when the model does not capture the observed increase in this variable. This effect is very likely caused by the formation of low-level clouds developing at night and dissipating after sunrise. This error, however, is not directly connected with the performance of the land surface scheme, whose assessment is the main focus of the present analysis. On the other hand, the model correctly reproduces the cloudy-sky conditions occurring on the fourth day, although without fully capturing its evolution in time, and in particular the gradual increase in incoming LW radiation.

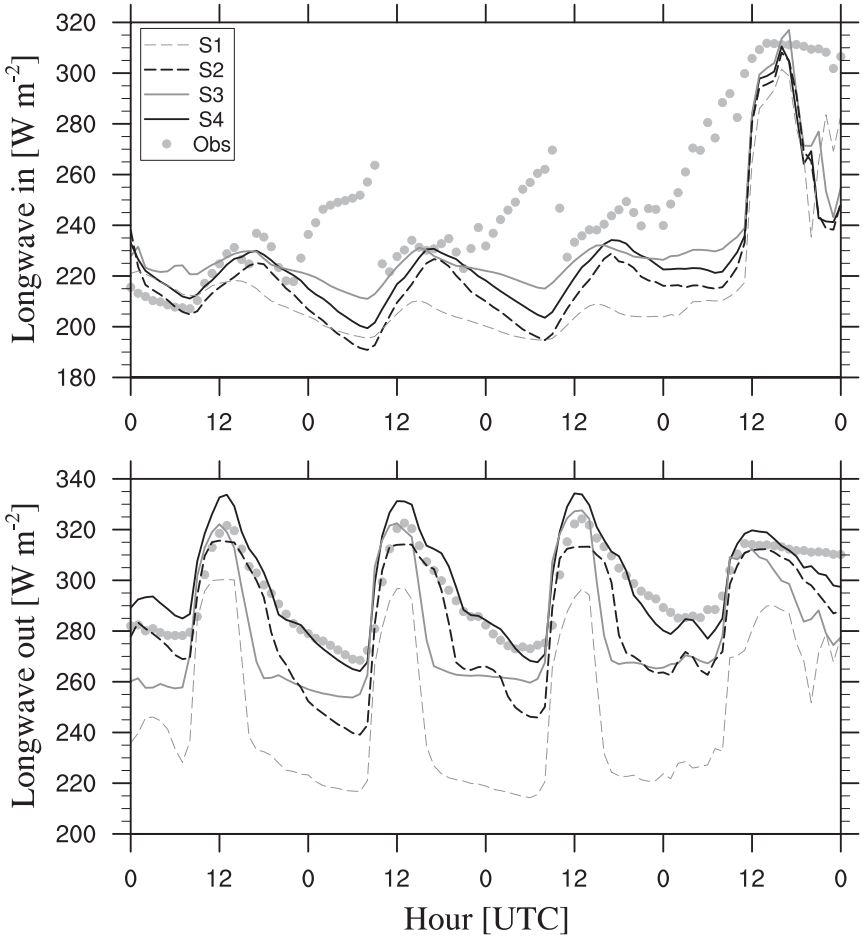

FIG. 4. Incoming and outgoing longwave radiation observed and estimated by the four simulations (S1–S4) at the valley floor reference station (AlRef).

The outgoing LW radiation is also better reproduced by the modified simulations. Simulation 3 properly identifies the daytime maxima. It still underestimates nighttime minima, but errors are strongly reduced with respect to simulation 1. Nevertheless, the rate of decrease in the outgoing LW radiation after sunset looks very different from observations: the model, in fact, instead of a gradual decrease in the variable, produces an almost instantaneous drop and a constant pattern during nighttime. Simulation 4, instead, better reproduces the decaying phase of outgoing LW radiation, whereas midday maximum values are slightly overestimated.

b. Temperature

Simulations 1 and 2 display evident underestimates of 2-m temperature, both during daytime and nighttime (Fig. 5). Higher errors affect simulation 1, especially for temperature minima. This means that, without any modification, in the present case Noah_MP performs better than Noah. Nevertheless, the proposed modifications result in an even better agreement with observations, due to an increase in the simulated temperature. In fact, decreasing the outgoing SW radiation allows the surface energy budget to have a significant extra rate of energy, with a consequent increase in the 2-m temperature. In simulation 3, maxima are still underestimated by ~3°–4°C, while nighttime temperatures are slightly overestimated. The net effect of the implemented modifications in simulation 3 is therefore a significant decrease in the daily thermal range. Simulation 4 exhibits the best agreement with observations. Nighttime minima are well captured by the model, with a maximum absolute error of ~1°C, while daytime maxima get closer to observations, but still underestimate real values by ~3°–4°C. Notice that on the last day the maximum temperature is well identified (especially by simulation 3), while the temperature drop after sunset is slightly overestimated. However this error follows the underestimation of the cloud cover and does not depend on the LSM, as can be

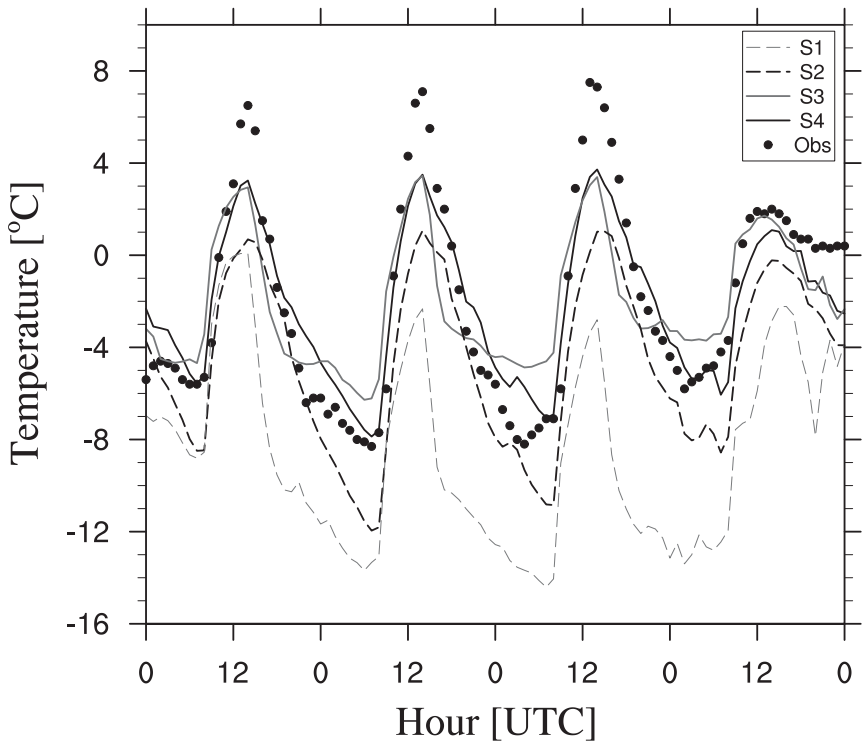

FIG. 5. The 2-m temperature observed and estimated by the four simulations (S1–S4) at the valley floor reference station (AlRef).

inferred also by the decrease in the incoming LW radiation in Fig. 4.

c. *Ground-based thermal inversion*

Some interesting considerations can be made regarding the model ability in reproducing the ground-based thermal inversion observed during the field campaign. Figures 6 and 7 show the 2-m temperature observed at the reference station of the valley floor (AlRef) and at the highest available station on the valley sidewalls (Sw1, 200 m above the valley floor). Data show a strong ground-based thermal inversion during nighttime, which systematically drops during daytime, due to the significant difference between the diurnal thermal range on the valley floor and on the sidewalls. Figure 6 shows that the inversion phenomenon is poorly reproduced when using Noah LSM, both before and after the modifications. While simulation 1 results in a too strong inversion during nighttime and barely identifies its decay during daytime, simulation 3 is able to increase daytime temperature more on the valley floor than along the sidewalls, but completely misses the thermal inversion during nighttime, except for a weak inversion on the second night. Conversely, WRF coupled with the Noah_MP scheme better reproduces the evolution of the thermal inversion, both in the standard and in the modified version (Fig. 7): simulation 2 can properly identify the nighttime inversion and slightly captures its morning breakup; the proposed modifications allow a stronger increase in the daytime 2-m temperature and therefore result in a more accurate reconstruction of the evolution in time of the thermal inversion.

d. *Statistical analysis*

To summarize the performance of the model in its different configurations, a statistical analysis on the results is presented. The analysis is performed comparing the model results against the observed time series of 2-m temperature, available at 9 different stations within the domain (see Fig. 1), and of downward and upward LW radiation and upward SW radiation at the reference station AlRef. Incoming SW radiation is not taken into account in this analysis as it is not affected by the modifications of the LSMs.

In the following, the values of different statistical indexes are discussed. First, the average model prediction errors are evaluated, analyzing the root-mean-square error (RMSE) and the bias (BIAS) values. Second, the mean-centered pattern errors are discussed by means of

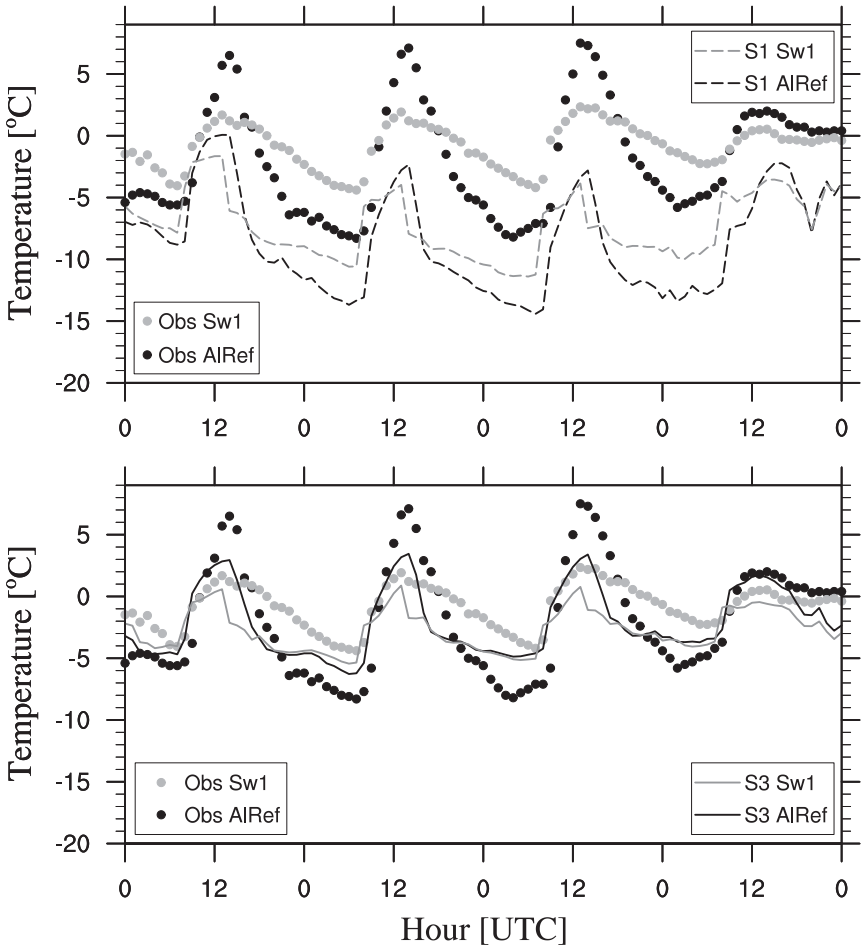

FIG. 6. Comparison of 2-m temperature at the valley floor and on the sidewall, observed and estimated with simulation 1 (standard Noah LSM) and simulation 3 (modified Noah LSM).

the Taylor diagrams (Taylor 2001). The Taylor diagram summarizes the performance of the model against the observations on the basis of the correlation coefficients R, the normalized centered root-mean-square differences E'_n, and the normalized standard deviations σ_{Mn}, which are second-order statistics calculated subtracting the average value from the time series. Equations (3)–(8) report the definition of each statistical index, where M_i and O_i are the modeled and observed values, N is the total number of values in the analyzed time series, and $\overline{O}$ and $\overline{M}$ are the observed and modeled averages, respectively:

$$\mathrm{RMSE} = \sqrt{\frac{1}{N}\sum_{i=1}^{N}(M_i - O_i)^2}, \tag{3}$$

$$\mathrm{BIAS} = \overline{O} - \overline{M}, \tag{4}$$

$$\sigma_O^2 = \frac{1}{N}\sum_{i=1}^{N}(O_i - \overline{O})^2, \tag{5}$$

$$R = \frac{\sum_{i=1}^{N}[(O_i - \overline{O})(M_i - \overline{M})]}{N\sigma_O\sigma_M}, \tag{6}$$

$$\sigma_{Mn}^2 = \frac{\sigma_M^2}{\sigma_O^2} = \frac{\sum_{i=1}^{N}(M_i - \overline{M})^2}{N\sigma_O^2}, \tag{7}$$

$$E_n'^2 = \frac{E'^2}{\sigma_O^2} = \frac{\sum_{i=1}^{N}[(O_i - \overline{O}) - (M_i - \overline{M})]^2}{N\sigma_O^2}. \tag{8}$$

Results from the comparison between measured and calculated 2-m temperatures are shown in Table 3 in terms of RMSE and BIAS. Values clearly show that the trend identified for the reference station is similar also for all the other stations: RMSE decreases from simulation 1 to simulation 4. In fact, in simulation 1 RMSE ranges from ~7° to ~8.7°C, in simulation 2 it assumes values of ~3.5°C, in simulation 3 it decays to ~2°C while in simulation 4 it reaches values ranging from 1.4° to

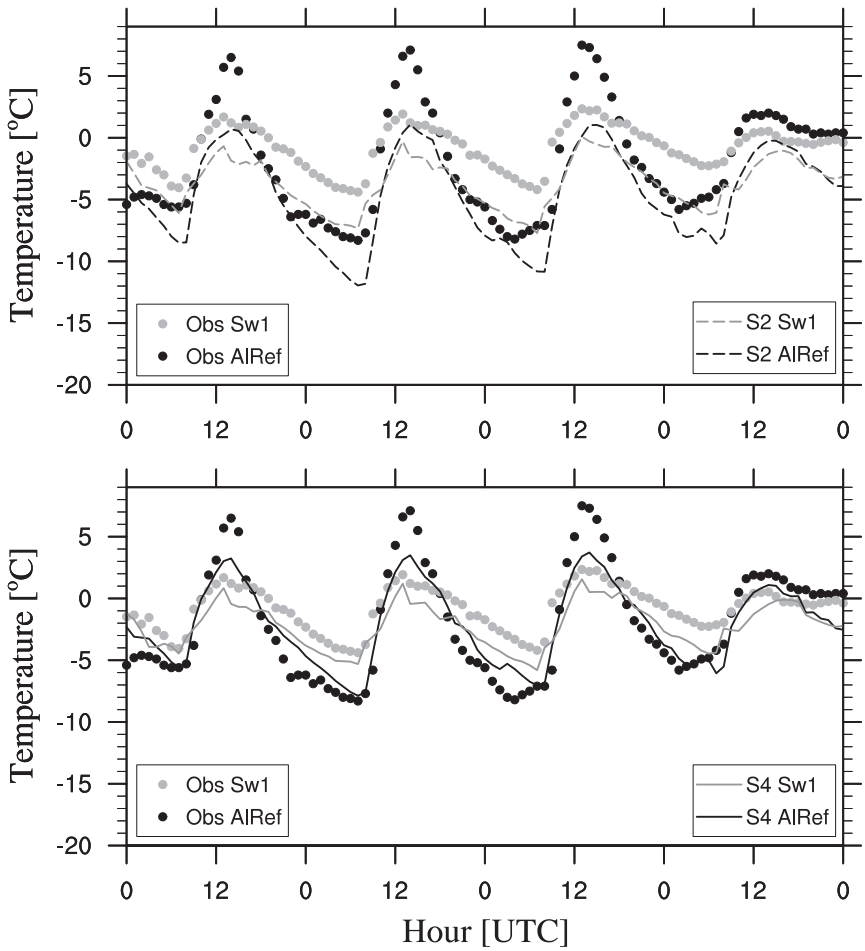

FIG. 7. Comparison of 2-m temperature at the valley floor and on the sidewall, observed and estimated with simulation 2 (standard Noah_MP LSM) and simulation 4 (modified Noah_MP LSM).

2.1°C. The BIAS values are generally positive, identifying an underestimation of the mean 2-m temperature in all the weather stations and they also confirm the improvements obtained with the modified simulations with respect to the standard simulations. The BIAS values obtained in simulation 4 are slightly higher than in simulation 3: indeed, overestimation of minima during nighttime and underestimation of daily peaks in simulation 3 tend to compensate each other, decreasing the resulting BIAS.

It is interesting to note that station Rov displays the highest RMSE and BIAS values in both the standard runs and higher indexes in simulation 4 than in simulation 3. This can be explained by considering the particular location of this weather station, which is situated in a rural area, but very close to the Rovereto city center. This location may influence the observations, as the urban heat island (Giovannini et al. 2011) affects the 2-m temperature nocturnal minima, which are higher than at all the other stations. The highest RMSE values of simulation 1 and 2 at Rov are then associated with the stronger underestimation of nocturnal temperature produced by the urban heat island. Accordingly, simulation 3, which tends to overestimate nighttime minima, performs better in this specific point. In principle, the effects determined by urban centers could be taken into account in the WRF Model by selecting an urban parameterization, but none of them is compatible with Noah_MP LSM and none was therefore applied in the present simulations.

Table 4 presents RMSE and BIAS for the radiation time series modeled and observed. The outgoing SW radiation presents high errors in both simulations 1 and 2, which are strongly reduced with the applied modifications. The RMSE is more than halved and the BIAS reaches smaller values, always negative, indicating a slight overestimation. A similar trend is found for the outgoing LW radiation, but, in this case, the variable is

TABLE 3. Statistical indexes calculated for 2-m temperature time series available at 9 different weather stations: root-mean-square error (RMSE) and bias (BIAS).

		RMSE (°C)				BIAS (°C)			
No.	Station	S1	S2	S3	S4	S1	S2	S3	S4
1	AlRef	7.22	3.12	2.36	1.70	6.63	2.68	0.14	0.18
2	Al1	8.10	3.90	2.20	1.69	7.59	3.67	0.74	1.18
3	Al2	7.52	3.25	2.23	1.45	6.91	2.95	0.29	0.47
4	Al3	7.54	3.58	1.92	1.80	7.09	3.11	0.57	0.77
5	Ronc	7.53	3.62	2.16	2.08	6.97	2.95	0.72	0.58
6	TNS	7.83	3.13	2.33	1.55	7.23	2.68	−0.48	−0.03
7	Rov	8.73	4.60	1.84	2.12	8.33	4.28	1.04	1.78
8	Sw1	7.63	3.69	2.41	1.81	7.09	3.54	1.65	1.60
9	Sw2	6.85	2.93	2.27	1.50	6.45	2.82	1.88	1.35
	Mean	7.66	3.54	2.19	1.75	7.14	3.19	0.73	0.88

underestimated. Improvements are smaller for the incoming LW radiation, because, as said before, this variable is only marginally and indirectly affected by the modifications of the LSMs.

In the Taylor diagrams presented in Fig. 8, R is related to the azimuthal angle, E'_n is proportional to the distance of the dots from the "OBS" point on the x axis, and σ_{Mn} is proportional to the radial distance from the origin. The top-left panel shows that, considering 2-m temperature at all stations, the modifications applied to the Noah model contribute to increase the correlation and to decrease E'_n. The standard deviation of the observations is overestimated by the standard run, while it is underestimated by the modified run. Indeed, as shown in Fig. 5, simulation 1 presents a wide thermal range (around an underestimated mean temperature), while simulation 3 strongly reduces it. The top-right panel shows that 2-m temperature time series calculated with the Noah_MP model are more grouped and lie closer to the curve of unitary normalized standard deviation. The thermal range is therefore better reproduced by the Noah_MP LSM than by the Noah model. The applied modifications contribute to further increase the correlation and to decrease E'_n but their effects are less effective than those obtained for the Noah simulations. Indeed, NoahMP performs better than Noah in its standard configuration and for this reason it is more difficult to further improve model results. A better performance of Noah_MP with respect to Noah was also found by Chen et al. (2014) and Kuribayashi et al. (2013), who assessed the ability of both models in simulating the snowpack evolution in time. The bottom panels of Fig. 8 present the Taylor diagrams for radiation time series. The graphics clearly show an improvement in both outgoing LW and SW radiation (especially from simulation 1), while the incoming LW radiation experiences slight changes only. The performance of the modified Noah and Noah_MP LSMs in predicting the radiation fluxes at the ground is in the end very similar, but yet the Noah_MP model better reproduces the 2-m temperature.

5. Discussion on the effects of each modification

To better highlight the influence on the model results of the different modifications implemented, Figs. 9 and 10 show the effects of each single modification on the outgoing SW and LW radiations and on the 2-m temperature. Figure 9 presents the effects of the modifications on the Noah simulations, providing an overview of the evolution from the standard simulation 1 to simulation 3. On the other hand, Fig. 10 shows the effects of the modifications on the Noah_MP simulations, highlighting the evolution from the standard simulation 2 to simulation 4. Therefore, the first intermediate step shown in Figs. 9 and 10 results from simulations run with only the modification to the land-use description, while the second intermediate step is from simulations run with coupled land-use and snow initialization modifications.

Focusing on simulations using Noah, Fig. 9 shows that an important decrease in the outgoing SW radiation is due to the modifications of land-use type, of initial snow cover, as well as to the implementation of the Livneh formula. In fact, cell albedo is a function of both snow cover fraction and vegetation land-use type: the modification of land-use type and of snow cover initialization has an impact on the cell snow cover fraction, decreasing with the change in land-use parameters and snow depth, while the modification to the implementation of the Livneh formula directly reduces the snow albedo. Furthermore each proposed modification has a significant impact on the 2-m temperature, increasing both nighttime minima and daytime maxima. In terms of 2-m temperature, the most significant effects arise from the decrease in the initial snow cover

TABLE 4. Statistical indexes calculated for the radiation time series available at the reference station AlRef: outgoing long- and shortwave radiation (LWout and SWout) and incoming longwave radiation (LWin). Root-mean-square error (RMSE) and bias (BIAS).

	RMSE (W m^{-2})				BIAS (W m^{-2})			
Variable	S1	S2	S3	S4	S1	S2	S3	S4
Swout	109.88	50.99	23.48	22.67	−59.08	−26.19	−11.85	−11.07
Lwout	52.18	17.11	21.29	8.37	32.69	27.65	16.69	21.7
Lwin	39.87	36.3	26.49	31.64	48.44	13.03	15.65	−2.81

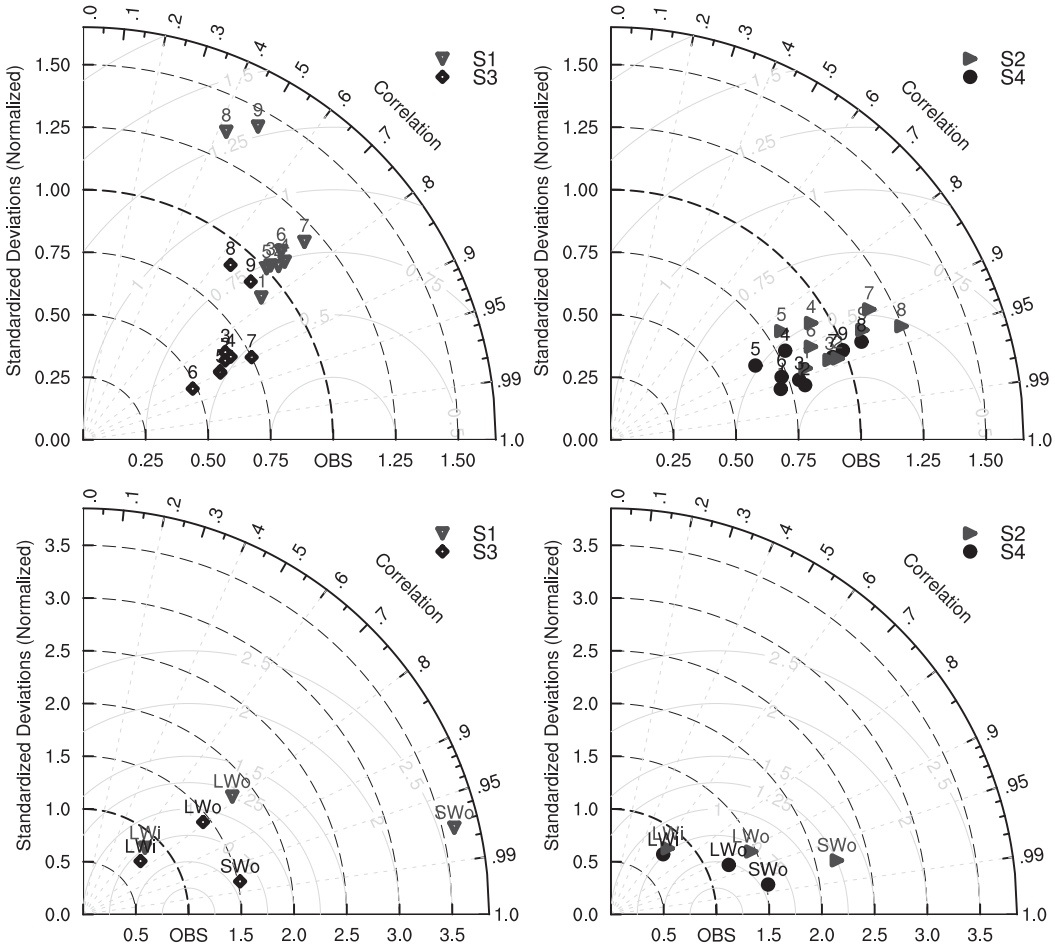

FIG. 8. Taylor diagrams describing the statistical patterns of the modeled 2-m temperature and radiation time series computed by simulations 1, 2, 3, and 4 with respect to the observations. (top) Results in terms of 2-m temperature, for each available weather station (from 1 to 9); (bottom) results in terms of outgoing LW (LWo) and SW (SWo) radiation and incoming LW (LWi) radiation. (left) Noah simulations S1 and S3 and (right) Noah_MP simulations S2 and S4.

height and from the changes in the implementation of the Livneh formula. It is interesting to note that the reduction of snow height in the simulation does have relevant positive effects in increasing the 2-m temperature even if the cell albedo does not strongly decrease: indeed, snow height reduction directly affects the calculation of the skin temperature (at the interface between the ground and the snow, if present), which tends to increase over a thinner snow cover; in addition to this, a thinner snow cover implies a different calculation of surface fluxes, especially the net upward heat flux. As 2-m temperature is calculated as a function of both the skin temperature and the surface heat flux, it is strongly affected by the modification of the initial snow depth. Figure 9 also shows that the major effect of the implemented modifications is a positive temperature shift, while the shape of the diurnal cycles is mostly preserved. In particular, in all cases Noah simulates a too fast decrease in the air temperature after sunset, probably due to a too fast decrease in the surface temperature, as also suggested by the rapid decrease in the outgoing LW radiation.

Noah_MP responds in a different way to the modifications (Fig. 10). Modifications to the land-use classification help in decreasing the outgoing SW radiation thanks to the presence of vegetation arising from the snow cover, which does not influence the SCF but directly influences the calculation of the cell albedo. This affects the 2-m temperature also, which slightly increases during daytime. The modification regarding the snow cover initialization intervenes again in reducing the cell albedo as the SCF decreases together with the snow depth as shown in Eq. (1). Accordingly, the 2-m temperature experiences an increase during both daytime and nighttime. Finally, eliminating the

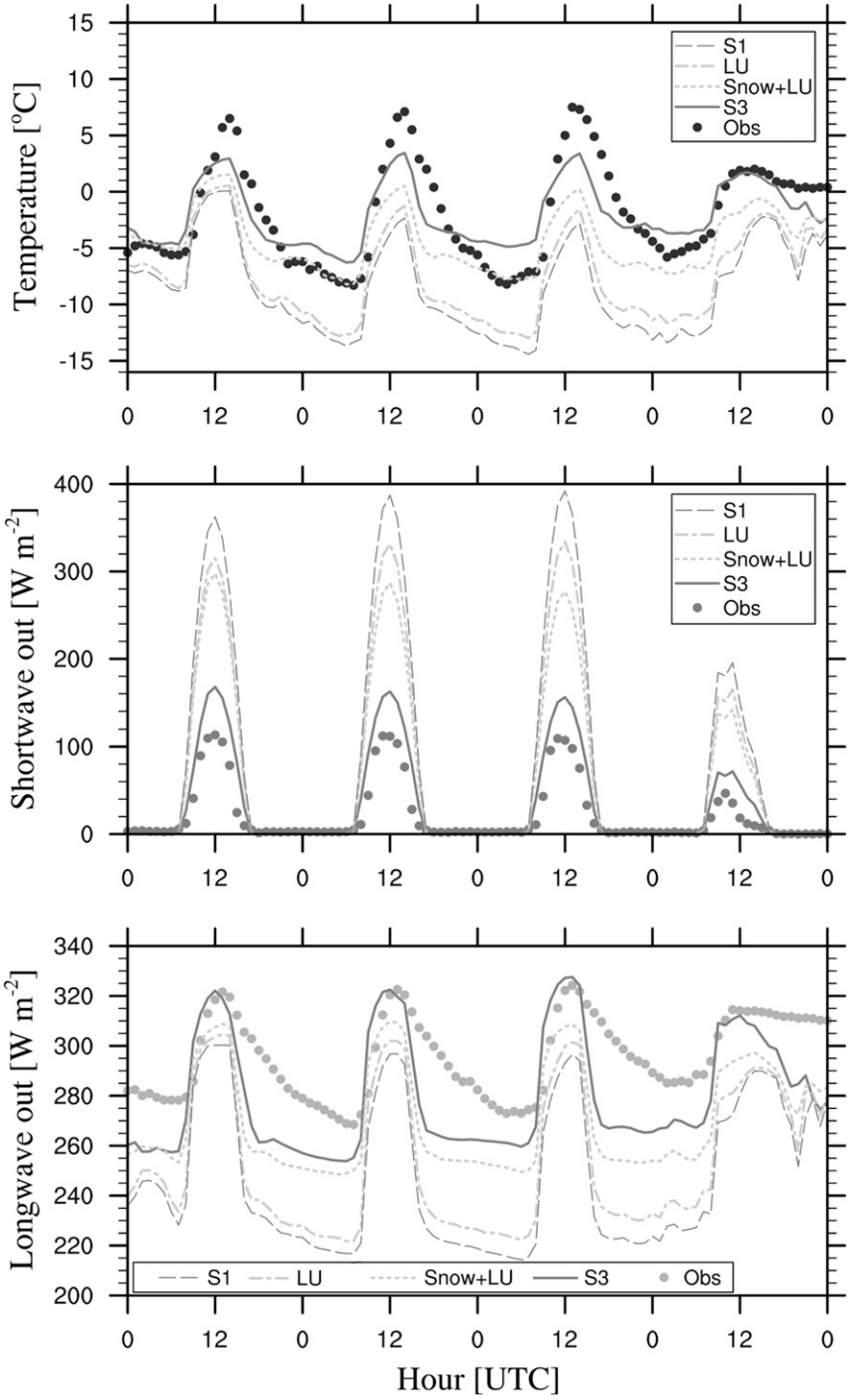

FIG. 9. The 2-m temperature and outgoing short- and longwave radiation observed and estimated adding one by one the proposed modifications, moving from simulation 1 (standard Noah LSM) to simulation 3 (modified Noah LSM): "Snow" refers to the modification applied to WRF snow cover initialization and "LU" refers to the modification to the land-use classification.

snow height threshold over which ground temperature cannot increase above 0°C causes a slight increase in the daily maxima on the first two days. It is interesting to notice that the modified simulations slightly overestimate the outgoing LW radiation at midday ($\sim 10\,\mathrm{W\,m^{-2}}$). This overestimation implies, using the Stefan–Boltzmann's law, an overestimation of skin temperature of ~2°C. Nonetheless, midday 2-m temperature

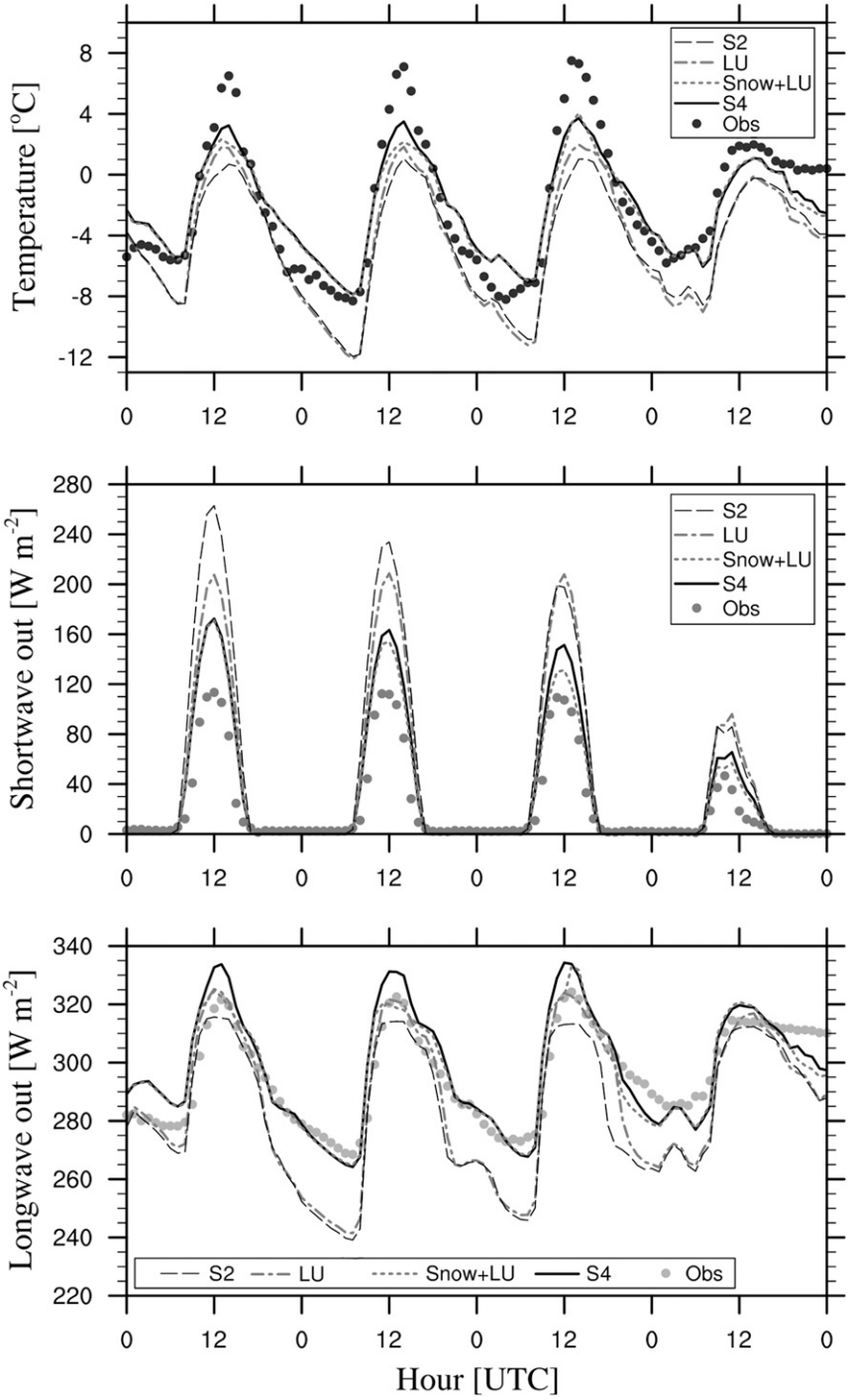

FIG. 10. The 2-m temperature and outgoing short- and longwave radiation observed and estimated adding one by one the proposed modifications, moving from simulation 2 (standard Noah_MP LSM) to simulation 4 (modified Noah_MP LSM): ''Snow'' refers to the modification applied to WRF snow cover initialization and ''LU'' refers to the modification to the land-use classification.

is yet underestimated: this fact implies that in the model the turbulence is overdamped during the day.

The above discussion highlights that both the Noah and Noah_MP LSMs are sensitive to very similar parameters, such as the initial snow depth, the land-use-type description, and the characteristics of the snowpack. In this case study, the Noah_MP LSM turns out to be the best performing scheme. The reasons for this better performance are primarily the improvements introduced in Noah_MP to reproduce the vegetation canopy layer, to calculate separately the vegetated and the bare ground surface temperatures, and to treat the snowpack. Indeed, other Noah_MP features were not tested here (e.g., no growing season is analyzed and therefore no new approaches on growing canopy are applied). Nevertheless, further accuracy is achieved by calibrating specific parameters of the model, such as the melting factor m and the land-use cover description parameters, in order to better fit the scale of the simulation and the characteristics of the investigated area. In conclusion, even though this case study takes advantage of few of the new features of Noah_MP, better results in both 2-m temperatures and outgoing SW radiation are achieved, if compared with the Noah LSM.

6. Conclusions and outlook

High-resolution numerical simulations with the WRF Model were performed to assess the performance of the Noah and Noah_MP LSMs over snow-covered ground in an Alpine valley. The two LSMs were evaluated by comparing their results against observations from a wintertime field campaign in the Adige valley, in the Italian Alps. As the aim of the present work was primarily the evaluation of the LSMs, comparisons were made in terms of 2-m temperature, both on the valley floor and on the sidewalls, and of incoming and outgoing SW and LW radiation in a reference station on the valley floor. Results from simulations using the default version of WRF, coupled with the two LSMs, highlighted a significant underestimation of the 2-m temperature and an overestimation of the outgoing SW radiation, due to an overestimation of the surface albedo. Given these results, both LSMs were analyzed in detail, in order to understand the possible causes of the recorded deficiencies. The first cause turned out to reside, in the present case, in the initialization of the snow cover depth, which was greatly overestimated. Another important role was played by the treatment of certain land-use classes under snow-covered ground. In particular, the IGBP class ''cropland'' is not representative of fruit tree cultures, which actually respond to a snow cover more like a broadleaf forest than like a cropland, which would be completely covered even under a thin snow layer. In addition to these corrections, other modifications were proposed, directly affecting the calculation of the cell albedo and of the 2-m temperature of both LSMs. In the Noah LSM modifications were introduced in the implementation of the Livneh procedure, in order to change the surface albedo calculation by intervening on the initial snow cover age and on the seasonal parameters describing the ground snow albedo evolution over time. In the Noah_MP scheme, changes were made in the snow cover upper limit, above which ground temperature cannot increase above 0°C.

Thanks to the applied modifications, improved results were obtained for both of the LSMs tested. In particular, in the modified simulations the outgoing SW radiation decreased, thus increasing the energy available in the surface energy budget, with a consequent increase in the 2-m temperature. Modifications had stronger impact on Noah LSM results. Nevertheless, the best agreement with observations was achieved with the modified Noah_MP LSM. Indeed, Noah_MP was able to properly catch nighttime temperature minima. Also, it can get closer to daytime maxima and to properly identify the nighttime ground-based thermal inversion and its evolution in time. All these improvements were quantitatively evaluated with a statistical analysis, which showed lowest RMSE and BIAS, and best agreement of the centered patterns with the observations for the modified simulations.

Results highlighted that particular attention must be paid to snow cover initialization when running wintertime simulations over complex terrain. This can be crucial for obtaining reliable results in these conditions, as accurate snow cover data are usually not available for high-resolution simulations, and the treatment of global reanalysis data may turn out to be misleading over complex terrain. Moreover, an appropriate land-use classification and description turned out to be very important for the calculation of the actual snow cover on the ground, with a considerable impact on the near-surface temperature. The calibration of the melting factor m also resulted to be significant in order to obtain an accurate estimate of the surface albedo through the calculation of a realistic value for the SCF. In simulations run at local scale, with a description of land cover types with a very high resolution, the value of m fixed within the Noah_MP model can lead to a severe underestimation of SCF and a consequent possible underestimation of surface albedo.

Modifications applied to the Noah scheme are also relevant, significantly improving the model performance. Moreover, these modifications are easy to introduce within the code, as the only parameters needed

are the age of the snow present on the ground at the beginning of the simulation and the season of the year. The modification proposed for the Noah_MP scheme regarding the calculation of surface temperature had actually less effect on the 2-m temperature if applied after the corrections to the snow initialization and to the land-use classification, resulting essentially in an increase in the maximum temperature. Nevertheless, this modification is more significant if applied when the cell presents no vegetated fraction.

It must be stressed, however, that the applied modifications have been tested only for this case study, and further testing over longer periods is needed in order to generalize their potential applicability in different regions and snowmelting conditions. Unfortunately, in this study, no measured data of snow depth were available in order to perform a direct comparison of model results against observations: for this reason testing against datasets with detailed snow-height observations would be of essential importance in order to highlight the effectiveness of the presented results. Nonetheless this work shows that the values of a few land surface parameters greatly influence model results and that an optimization of some of them can make the difference in applications over complex terrain. A refinement in the estimation of surface variables and of their effects in the evaluation of surface layer processes is of utmost importance for situations involving strong interactions of the surface with the lower atmosphere. An accurate simulation of quantities such as surface layer turbulence, near-surface stability, and surface layer height are key prerequisites for many applications, such as pollutant dispersion modeling in mountain valleys and basins. Indeed, the proposed improvements are expected to lead to better performance of WRF in providing a meteorological input for pollutant dispersion models, especially with the high resolution available from increasingly powerful computational resources, and required by very complex terrain situations (Giovannini et al. 2014b, 2017; Ragazzi et al. 2013).

Acknowledgments. Special thanks to Prof. Enrico Ferrero for his valuable suggestions and help in developing the statistical analysis for this paper. Meteotrentino, the Meteorological Office of the Autonomous Province of Trento, and the Edmund Mach Foundation are also kindly acknowledged for providing data from their permanent weather stations.

REFERENCES

Ball, J. T., I. E. Woodrow, and J. A. Berry, 1987: A model predicting stomatal conductance and its contribution to the control of photosynthesis under different environmental conditions. *Progress in Photosynthesis Research*, J. Biggins, Ed., Vol. 4, Springer, 221–224, doi:10.1007/978-94-017-0519-6_48.

Barlage, M., and Coauthors, 2010: Noah land surface model modifications to improve snowpack prediction in the Colorado Rocky Mountains. *J. Geophys. Res.*, **115**, D22101, doi:10.1029/2009JD013470.

Bonan, G. B., 1996: A land surface model (LSM version 1.0) for ecological, hydrological, and atmospheric studies: Technical description and user's guide. NCAR Tech. Note NCAR/TN-417+STR, National Center for Atmospheric Research, Boulder, CO, 150 pp.

Chen, F., and J. Dudhia, 2001: Coupling an advanced land surface-hydrology model with the Penn State–NCAR MM5 modeling system. Part I: Model implementation and sensitivity. *Mon. Wea. Rev.*, **129**, 569–585, doi:10.1175/1520-0493(2001)129<0569:CAALSH>2.0.CO;2.

——, and Coauthors, 1996: Modeling of land surface evaporation by four schemes and comparison with FIFE observations. *J. Geophys. Res.*, **101**, 7251–7268, doi:10.1029/95JD02165.

——, and Coauthors, 2014: Modeling seasonal snowpack evolution in the complex terrain and forested Colorado Headwaters region: A model intercomparison study. *J. Geophys. Res. Atmos.*, **119**, 13 795–13 819, doi:10.1002/2014JD022167.

Collatz, G. J., J. T. Ball, C. Grivet, and J. A. Berry, 1991: Physiological and environmental regulation of stomatal conductance, photosynthesis and transpiration: A model that includes a laminar boundary layer. *Agric. For. Meteor.*, **54**, 107–136, doi:10.1016/0168-1923(91)90002-8.

——, M. Ribas-Carbo, and J. A. Berry, 1992: Coupled photosynthesis-stomatal conductance model for leaves of C_4 plants. *Aust. J. Plant Physiol.*, **19**, 519–538, doi:10.1071/PP9920519.

de Ferranti, J., 2013: 30-m topography dataset. Accessed March 2015, http://viewfinderpanoramas.org/.

de Franceschi, M., and D. Zardi, 2009: Study of wintertime high pollution episodes during the Brenner-South ALPNAP measurement campaign. *Meteor. Atmos. Phys.*, **103**, 237–250, doi:10.1007/s00703-008-0327-2.

Dirmeyer, P. A., X. Gao, M. Zhao, Z. Guo, T. Oki, and N. Hanasaki, 2006: SGSWP-2: Multimodel analysis and implications for our perception of the land surface. *Bull. Amer. Meteor. Soc.*, **87**, 1381–1397, doi:10.1175/BAMS-87-10-1381.

Dudhia, J., 1989: Numerical study of convection observed during the Winter Monsoon Experiment using a mesoscale two-dimensional model. *J. Atmos. Sci.*, **46**, 3077–3107, doi:10.1175/1520-0469(1989)046<3077:NSOCOD>2.0.CO;2.

Ek, M. B., K. E. Mitchell, Y. Lin, E. Rogers, P. Grunmann, V. Koren, G. Gayno, and J. D. Tarpley, 2003: Implementation of Noah land surface model advances in the National Centers for Environmental Prediction operational mesoscale Eta model. *J. Geophys. Res.*, **108**, 8851, doi:10.1029/2002JD003296.

European Environment Agency, 2006: 100-m landuse cover data. European Environment Agency, http://land.copernicus.eu/pan-european/corine-land-cover/clc-2006/view.

Giovannini, L., D. Zardi, and M. de Franceschi, 2011: Analysis of the urban thermal fingerprint of the city of Trento in the Alps. *J. Appl. Meteor. Climatol.*, **50**, 1145–1162, doi:10.1175/2010JAMC2613.1.

——, ——, ——, and F. Chen, 2014a: Numerical simulations of boundary-layer processes and urban-induced alterations in an Alpine valley. *Int. J. Climatol.*, **34**, 1111–1131, doi:10.1002/joc.3750.

——, G. Antonacci, D. Zardi, L. Laiti, and L. Panziera, 2014b: Sensitivity of simulated wind speed to spatial resolution over complex terrain. *Energy Procedia*, **59**, 323–329, doi:10.1016/j.egypro.2014.10.384.

——, L. Laiti, S. Serafin, and D. Zardi, 2017: The thermally driven diurnal wind system of the Adige Valley in the Italian Alps. *Quart. J. Roy. Meteor. Soc.*, **143**, 2389–2402, doi:10.1002/qj.3092.

Grell, G. A., and D. Dévényi, 2002: A generalized approach to parameterizing convection combining ensemble and data assimilation techniques. *Geophys. Res. Lett.*, **29**, doi:10.1029/2002GL015311.

Hall, D. K., and G. A. Riggs, 2016: MODIS/*Terra* snow cover daily L3 global 500m grid, version 6 [February 2006, Europe]. NASA National Snow and Ice Data Center Distributed Active Archive Center, Boulder, Colorado, accessed March 2017, doi:10.5067/MODIS/MOD10A1.006.

Heimann, D., and Coauthors, 2007: Air pollution, traffic noise and related health effects in the alpine space—A guide for authorities and consulters. ALPNAP Comprehensive Report. Tech. Rep., Department of Civil, Environmental and Mechanical Engineering, University of Trento, Trento, Italy, 335 pp., http://www.imk-ifu.kit.edu/downloads/institute/ALPNAP_electronic_version.pdf.

Hong, S.-Y., J. Dudhia, and S.-H. Chen, 2004: A revised approach to ice microphysical processes for the bulk parameterization of clouds and precipitation. *Mon. Wea. Rev.*, **132**, 103–120, doi:10.1175/1520-0493(2004)132<0103:ARATIM>2.0.CO;2.

——, Y. Noh, and J. Dudhia, 2006: A new vertical diffusion package with an explicit treatment of entrainment processes. *Mon. Wea. Rev.*, **134**, 2318–2341, doi:10.1175/MWR3199.1.

Jin, J., and N. L. Miller, 2007: Analysis of the impact of snow on daily weather variability in mountainous regions using MM5. *J. Hydrometeor.*, **8**, 245–258, doi:10.1175/JHM565.1.

——, ——, and N. Schlegel, 2010: Sensitivity study of four land surface schemes in the WRF Model. *Adv. Meteor.*, **2010**, 167436, doi:10.1155/2010/167436.

Jordan, R., 1991: A one-dimensional temperature model for a snow cover. Special Rep. SR 91-16, Cold Region Research and Engineering Lab., U.S. Army Corps. of Engineers, Hanover, NH, 61 pp.

Koren, V., J. Schaake, K. Mitchell, Q. Duan, F. Chen, and J. Baker, 1999: A parameterization of snowpack and frozen ground intended for NCEP weather and climate models. *J. Geophys. Res.*, **104**, 19 569–19 585, doi:10.1029/1999JD900232.

Kuribayashi, M., N. J. Noh, T. M. Saitoh, I. Tamagawa, Y. Wakazuki, and H. Muraoka, 2013: Comparison of snow water equivalent estimated in central Japan by high-resolution simulations using different land-surface models. *SOLA*, **9**, 148–152, doi:10.2151/sola.2013-033.

Livneh, B., Y. Xia, K. E. Mitchell, M. B. Ek, and D. P. Lettenmaier, 2010: Noah LSM snow model diagnostics and enhancements. *J. Hydrometeor.*, **11**, 721–738, doi:10.1175/2009JHM1174.1.

Mahrt, L., and M. Ek, 1984: The influence of atmospheric stability on potential evaporation. *J. Climate Appl. Meteor.*, **23**, 222–234, doi:10.1175/1520-0450(1984)023<0222:TIOASO>2.0.CO;2.

——, and H. L. Pan, 1984: A two-layer model of soil hydrology. *Bound.-Layer Meteor.*, **29**, 1–20, doi:10.1007/BF00119116.

Meloysund, V., B. Leira, K. V. Hoiseth, and K. R. Liso, 2007: Predicting snow density using meteorological data. *Meteor. Appl.*, **14**, 413–423, doi:10.1002/met.40.

Mlawer, E. J., S. J. Taubman, P. D. Brown, M. J. Iacono, and S. A. Clough, 1997: Radiative transfer for inhomogeneous atmospheres: RRTM, a validated correlated-k model for the longwave. *J. Geophys. Res.*, **102**, 16 663–16 682, doi:10.1029/97JD00237.

Niu, G.-Y., and Z.-L. Yang, 2006: Effects of frozen soil on snowmelt runoff and soil water storage at a continental scale. *J. Hydrometeor.*, **7**, 937–952, doi:10.1175/JHM538.1.

——, and ——, 2007: An observation-based formulation of snow cover fraction and its evaluation over large North American river basins. *J. Geophys. Res.*, **112**, D21101, doi:10.1029/2007JD008674.

——, ——, R. E. Dickinson, L. E. Gulden, and H. Su, 2007: Development of a simple groundwater model for use in climate models and evaluation with gravity recovery and climate experiment data. *J. Geophys. Res.*, **112**, D07103, doi:10.1029/2006JD007522.

——, and Coauthors, 2011: The community Noah land surface model with multiparameterization options (Noah_MP): 1. Model description and evaluation with local-scale measurements. *J. Geophys. Res.*, **116**, D12109, doi:10.1029/2010JD015139.

Noilhan, J., and S. Planton, 1989: A simple parameterization of land surface processes for meteorological models. *Mon. Wea. Rev.*, **117**, 536–549, doi:10.1175/1520-0493(1989)117<0536:ASPOLS>2.0.CO;2.

Oleson, K. W., and Coauthors, 2013: Technical description of version 4.5 of the Community Land Model (CLM). NCAR Tech. Note NCAR/TN-503+STR, National Center for Atmospheric Research, Boulder, CO, 422 pp., accessed February 2016, doi:10.5065/D6RR1W7M.

Pan, H.-L., and L. Mahrt, 1987: Interaction between soil hydrology and boundary-layer development. *Bound.-Layer Meteor.*, **38**, 185–202, doi:10.1007/BF00121563.

Pomeroy, J. W., and E. Brun, 2001: Physical properties of snow. *Snow Ecology: An Interdisciplinary Examination of Snow-Covered Ecosystems*, H. G. Jones et al., Eds., Cambridge University Press, 45–118.

Qu, X., and A. Hall, 2006: Assessing snow albedo feedback in simulated climate change. *J. Climate*, **19**, 2617–2630, doi:10.1175/JCLI3750.1.

Ragazzi, M., W. Tirler, G. Angelucci, D. Zardi, and E. Rada, 2013: Management of atmospheric pollutants from waste incineration processes: The case of Bozen. *Waste Manage. Res.*, **31**, 235–240, doi:10.1177/0734242X12472707.

Sakaguchi, K., and X. Zeng, 2009: Effects of soil wetness, plant litter, and under-canopy atmospheric stability on ground evaporation in the Community Land Model (CLM3.5). *J. Geophys. Res.*, **114**, D01107, doi:10.1029/2008JD010834.

Schaake, J. C., V. I. Koren, Q. Y. Duan, K. Mitchell, and F. Chen, 1996: A simple water balance model (SWB) for estimating runoff at different spatial and temporal scales. *J. Geophys. Res.*, **101**, 7461–7475, doi:10.1029/95JD02892.

Sellers, P. J., and Coauthors, 1996: A Revised Land Surface Parameterization (SiB2) for atmospheric GCMS. Part I: Model formulation. *J. Climate*, **9**, 676–705, doi:10.1175/1520-0442(1996)009<0676:ARLSPF>2.0.CO;2.

Skamarock, W. C., and Coauthors, 2008: A description of the Advanced Research WRF version 3. NCAR Tech. Note NCAR/TN-475+STR, 113 pp., http://dx.doi.org/10.5065/D68S4MVH.

Su, H., Z.-L. Yang, G.-Y. Niu, and R. Dickinson, 2008: Enhancing the estimation of continental-scale snow water equivalent by assimilating MODIS snow cover with the ensemble Kalman filter. *J. Geophys. Res.*, **113**, D08120, doi:10.1029/2007JD009232.

Taylor, K. E., 2001: Summarizing multiple aspects of model performance in a single diagram. *J. Geophys. Res.*, **106**, 7183–7192, doi:10.1029/2000JD900719.

Verseghy, D. L., 1991: Class—A Canadian land surface scheme for GCMS. I. Soil model. *Int. J. Climatol.*, **11**, 111–133, doi:10.1002/joc.3370110202.

Xue, Y., P. J. Sellers, J. L. Kinter, and J. Shukla, 1991: A simplified biosphere model for global climate studies. *J. Climate*, **4**, 345–364, doi:10.1175/1520-0442(1991)004<0345:ASBMFG>2.0.CO;2.

Yang, Z.-L., and Coauthors, 2011: The community Noah land surface model with multiparameterization options (Noah-MP): 2. Evaluation over global river basins. *J. Geophys. Res.*, **116**, D12110, doi:10.1029/2010JD015140.

Zängl, G., 2012: Extending the numerical stability limit of terrain-following coordinate models over steep slopes. *Mon. Wea. Rev.*, **140**, 3722–3733, doi:10.1175/MWR-D-12-00049.1.

Zhang, H., Z. Pu, and X. Zhang, 2013: Examination of errors in near-surface temperature and wind from WRF numerical simulations in regions of complex terrain. *Wea. Forecasting*, **28**, 893–914, doi:10.1175/WAF-D-12-00109.1.